ISSN (Print) 1226-1750
ISSN (Online) 2233-6656
Journal of Magnetics 31(3), 391-402 (2026) https://doi.org/10.4283/JMAG.2026.31.3.391

Residual-Correction Multi-Fidelity Surrogate Model Assisted Optimization of an Axial Flux Permanent Magnet Motor Using Q-3D and 3D FEM

In-Yeong Hwang and Dong-Kuk Lim*

Department of Electrical, Electronic and Computer Engineering, University of Ulsan, Ulsan 44610, Republic of Korea

(Received 10 August 2026, Received in final form 1 September 2026, Accepted 2 September 2026)

This study proposes a residual-correction (RC) multi-fidelity surrogate model consisting of two surrogate models. First, a quasi-three-dimensional finite element method (Q-3D) surrogate model is trained using many Q-3D samples to capture the overall performance trends. Second, a residual surrogate model is trained using small number of three-dimensional finite element method (3D FEM) samples to learn the difference between the Q-3D surrogate model predictions and 3D FEM results. The Q-3D and residual surrogate models are combined to accurately predict the 3D FEM results. The RC model is coupled with a genetic algorithm for optimization, and the optimized design is evaluated using 3D FEM. The average torque increases from 551.83 Nm for the initial model to 553.63 Nm for the optimized model. Meanwhile, the torque ripple decreases from 9.65 % to 6.66 %.

Keywords : axial flux permanent magnet motor, finite element method, multi-fidelity surrogate model, residual-correction, quasi-three-dimensional analysis

1. Introduction

Permanent magnet synchronous motors (PMSMs) can be classified into radial flux permanent magnet motors (RFPMs) and axial flux permanent magnet motors (AFPMs) according to the primary direction of magnetic flux. RFPMs have a cylindrical geometry, and their magnetic flux flows primarily in the radial direction. In RFPMs, the radial flux distribution can be considered approximately constant along the axial direction when axial end effects are neglected. Therefore, RFPMs can be analyzed using two-dimensional finite element method (2D FEM).

AFPMs are attractive for applications requiring high torque density [1-4]. Unlike RFPMs, AFPMs have a disc-shaped geometry, and their magnetic flux flows primarily in the axial direction. Because of this characteristic, the air gap flux distribution varies radially and cannot be accurately represented using 2D FEM. Therefore, accurate analysis of AFPM performance generally requires three-dimensional finite element method (3D FEM), which can account for the overall three-dimensional magnetic flux distribution [4-6]. Although 3D FEM can accurately evaluate the electromagnetic performance of AFPMs, it requires considerable computational cost [7-11]. To overcome this problem, quasi-three-dimensional (Q-3D) analysis has been studied as a computationally efficient alternative to 3D FEM.

In slice-based Q-3D, the AFPM is divided into several radial slices. Because the magnetic flux in AFPM flows primarily in the axial direction, each radial slice can be analyzed using 2D FEM to estimate the axial flux distribution. By combining the analysis results of the individual slices, Q-3D can approximate the overall motor performance with significantly reduced computational cost [12-17]. However, Q-3D is less accurate than 3D FEM because it neglects radial flux leakage and end-leakage effects [18, 19]. Therefore, there is a trade-off between accuracy and computational cost in 3D FEM and Q-3D.

Optimization requires repeated performance evaluations for many design candidates. Therefore, the high computational cost associated with repeated FEM evaluations can be reduced by replacing FEM with a surrogate model. A surrogate model is an approximate model that learns the relationship between the design variables and performance responses. However, a single-fidelity surrogate model relies on only one type of dataset, such as Q-3D or 3D FEM data. Consequently, a Q-3D based single-fidelity surrogate model may exhibit differences from 3D FEM

©The Korean Magnetics Society. All rights reserved.
*Corresponding author: Tel: +82-52-259-1072
E-mail: ldk8745@ulsan.ac.kr

© 2026 Journal of Magnetics

results, whereas a 3D FEM-based single-fidelity surrogate model requires a high computational cost to generate the training data.

To address this problem, multi-fidelity transfer learning (TL) has been studied. Multi-fidelity methods combine low- and high-fidelity data with different levels of accuracy and computational cost to achieve high prediction accuracy while reducing computational cost. In TL, first, a low-fidelity dataset with many samples is used to pre-train the surrogate model to capture the overall response trends. Second, a high-fidelity dataset with small number of samples is used to fine-tune the pre-trained surrogate model and improve its prediction accuracy [23-25]. [23] combined 2D FEM and 3D FEM data using TL for electrical machine design, thereby reducing the dependence on computationally expensive 3D FEM. Similarly, [24] employed low cost 2D FEM data together with a limited number of 3D FEM samples to account for three-dimensional electromagnetic effects with reduced computational cost. [25] also demonstrated that TL using low- and high-fidelity FEM data can improve the efficiency of high-fidelity performance prediction. By applying TL, the surrogate model can achieve high prediction accuracy with reduced computational cost. However, when offsets exist between the low- and high-fidelity responses, fine-tuning with small number of high-fidelity samples may not fully correct these differences while preserving the response relationship learned from the low-fidelity data. Because TL gradually updates the parameters pre-trained on the low-fidelity data using small number of high-fidelity samples, the fine-tuning process may not sufficiently correct a large offset between the low- and high-fidelity data.

To address this issue, this study proposes a residual-correction (RC) model. The RC model training workflow is shown in Fig. 1. First, the surrogate model is trained using Q-3D data to capture global trends. Second, a separate residual surrogate model is trained to learn the difference between the Q-3D based surrogate model predictions and the 3D FEM results for the same inputs. Finally, the outputs of the Q-3D and residual surrogate models are combined to obtain the final high-fidelity prediction. The RC model directly learns the differences between the Q-3D surrogate predictions and 3D FEM results, rather than correcting the low-fidelity model through parameter fine-tuning.

The proposed RC model is compared with single-fidelity and TL surrogate models. Finally, the trained RC model is coupled with a genetic algorithm (GA) to obtain the optimal design. The optimal design is analyzed using 3D FEM to evaluate the accuracy of the RC model at the selected design.

The main contribution of this study is a Q-3D to 3D FEM multi-fidelity framework in which a DNN trained on inexpensive Q-3D data is retained as the base model, while a separate DNN explicitly learns the model-level residual from a limited number of 3D FEM samples. Second, the proposed RC model is compared with Q-3D-only, 3D FEM-only, and transfer-learning surrogate models using the same independent 3D FEM test set to evaluate its prediction performance. Third, the trained RC model is coupled with a GA for the optimal design of an AFPM, and the selected optimal design is finally evaluated using 3D FEM.

2. Analysis Method of AFPM

2.1. Target AFPM

Fig. 2 shows the geometry of the target AFPM and the locations of the five design variables, while the main geometric specifications are summarized in Table 1. Table 2 lists the initial values and design ranges of the five variables, which define the design space considered in the optimization. The rated operating conditions and per-

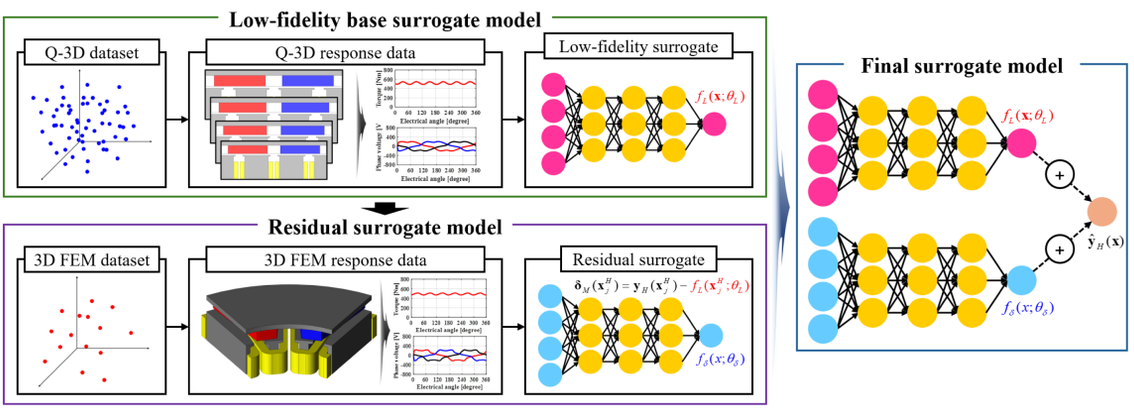


Fig. 1. (Color online) Training workflow of the proposed residual-correction multi-fidelity surrogate model.

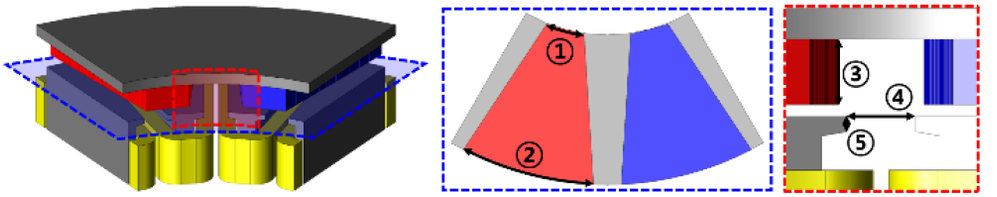


Fig. 2. (Color online) Geometry of the target AFPM and definitions of the five design variables: ① inner magnet arc ratio, ② outer magnet arc ratio, ③ magnet thickness, ④ slot-opening width, and ⑤ shoe thickness.

Table 1. Main geometric specifications of the target AFPM.

Specification	Value
Number of poles / slots	12 / 18
Inner diameter [mm]	110
Outer diameter [mm]	220
Air gap [mm]	1.5

formance targets are summarized in Table 3. The rated torque and torque ripple targets are set to 550 Nm and 8 %, respectively, and these values are used as the performance requirements for evaluating the candidate designs.

2.2. 3D FEM Analysis

In an AFPM, the magnetic flux flows primarily in the axial direction, causing the electromagnetic field distribution to vary radially. Therefore, conventional 2D FEM cannot accurately represent these radial variations in the axial magnetic flux, whereas 3D FEM can consider the overall three-dimensional magnetic flux distribution. However, 3D FEM requires many mesh elements and degrees of freedom because the entire three-dimensional geometry must be divided into finite elements. Therefore, the size of the system equations and the computational cost of each analysis increase significantly. Consequently, 3D FEM provides high accuracy but requires considerable computational cost.

2.3. Q-3D Analysis

The slicing method of Q-3D is illustrated in Fig. 3.

Table 3. Rated operating conditions and performance targets.

Performance	Value
Rated speed [rpm]	2,000
Rated torque [Nm]	550
Rated power [kW]	115
Rated torque ripple [%]	8
Magnet usage [mm^3]	339,888

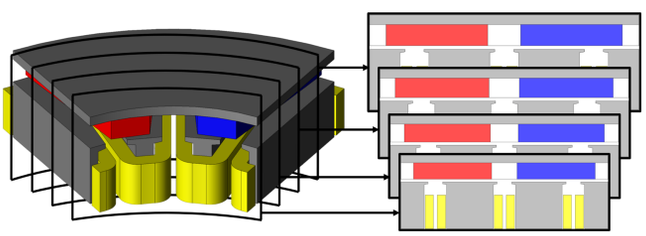


Fig. 3. (Color online) Q-3D slicing procedure.

Unlike conventional 2D FEM, the AFPM model is divided into N_s slices at equal intervals along the radial direction [12-15]. Because the AFPM is divided along the radial direction, each slice can be used to estimate the axial magnetic flux at the corresponding radial position. Each radial slice is then unwrapped and flattened into an equivalent linear motor model.

The electromagnetic force is calculated for each slice, and the torque contribution of each slice is obtained by multiplying the electromagnetic force by the corresponding radius. The torque contributions from all slices are then summed to estimate the overall AFPM performance. The torque contribution of the *i*-th slice is calculated as

Table 2. Initial values and design range of the five design variables.

Number	Variable	Initial value	Minimum range	Maximum range
①	α_{inner}	0.45	0.35	0.6
②	α_{outer}	0.83	0.7	0.95
③	m_{thick} [mm]	8.5	7.5	9.5
④	w_{slot} [mm]	9	6	11
⑤	t_{shoe} [mm]	2	1	3

Table 4. Convergence of Q-3D average torque and torque ripple with respect to the number of radial slices.

Number of slices	Average torque [Nm]	Relative change [%]	Torque ripple [%]	Absolute change [%$_p$]
1	601.74	-	18.71	-
3	582.38	-3.22	10.52	-8.19
5	580.91	-0.25	10.09	-0.43
7	580.54	-0.06	10.04	-0.05

$$T_i = r_i \times F_i \tag{1}$$

Here, r_i is the representative radius and F_i is the corresponding electromagnetic force of the i-th slice. The total torque is approximated by summing the torque contributions of all slices:

$$T_{total} = \sum_{i=1}^{N_s} T_i \tag{2}$$

Compared with 3D FEM, Q-3D significantly reduces the computational cost by replacing the three-dimensional model with multiple 2D slice models that require fewer mesh elements and degrees of freedom [14-17]. However, this simplification into independent two-dimensional slices reduces the accuracy of Q-3D compared with 3D FEM.

2.4. Q-3D Convergence and Fidelity-Gap Analysis

In this study, the number of Q-3D slices was determined through a convergence study by gradually increasing the number of slices and comparing the electromagnetic performance. Table 4 summarizes the Q-3D average torque and torque ripple for different numbers of slices. Based on these results, the minimum number of slices was selected considering both Q-3D accuracy and computational cost. As a result, seven slices were selected because the relative changes in average torque and torque ripple from the previous case were less than 0.1 % and 0.1 %$_p$, respectively.

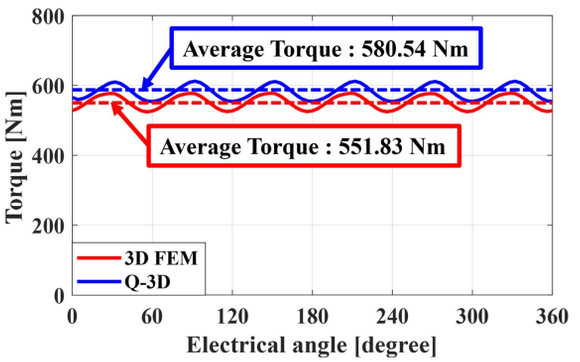


Fig. 4. (Color online) Torque waveforms obtained using Q-3D and 3D FEM at the rated operating point.

Table 5. Comparison of Q-3D and 3D FEM results and computational times at the rated operating point.

Value	3D FEM	Q-3D	Difference
Average torque [Nm]	551.83	580.54	5.20 [%]
Torque ripple [%]	9.65	10.04	0.39 [%$_p$]
Time [s]	3,688	168	-95.44 [%]

In this section, Q-3D and 3D FEM are compared to investigate the differences and relationship between the two methods. At the rated operating point, Fig. 4 shows the torque waveforms obtained using Q-3D and 3D FEM. As summarized in Table 5, Q-3D overestimates the average torque obtained from 3D FEM by 5.20 %, whereas the torque ripple values differ by only 0.39 %$_p$. In terms of computation time, a single Q-3D analysis requires 168 s, compared with 3,688 s for 3D FEM, corresponding to a 95.44 % reduction.

Fig. 5 and 6 compare the Q-3D and 3D FEM results obtained by changing each design variable, and the corresponding correlation coefficients are summarized in Table 6. In Q-3D analysis, the 3D AFPM geometry is approximated by combining independently analyzed 2D radial slices. Therefore, interactions between adjacent slices, radial electromagnetic-field variations, and end-leakage effects are not fully represented. As a result, Q-3D analysis may overestimate the average torque compared with 3D FEM [18, 19].

In addition, the Q-3D model reproduces the 3D FEM torque ripple trends for the slot-opening width and shoe thickness less accurately than magnet-related design variables. Previous studies have shown that stator tooth geometry and permanent magnet configuration can significantly affect cogging torque in axial-flux PM machines [20, 21]. In addition, air gap flux density harmonics are closely related to cogging torque and torque ripple [22]. These geometric variables affect local air-gap field harmonics, which can contribute to torque ripple variation. Therefore, the low correlations for slot-opening width and shoe thickness may be associated with

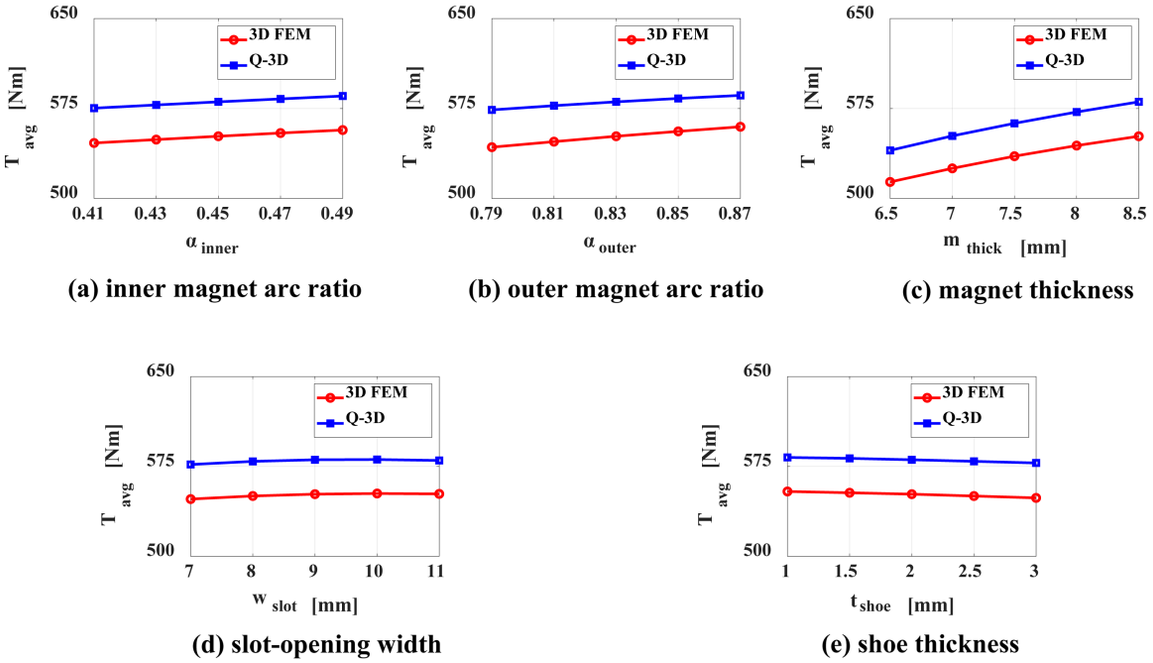


Fig. 5. (Color online) Comparison of average torque obtained using Q-3D and 3D FEM.

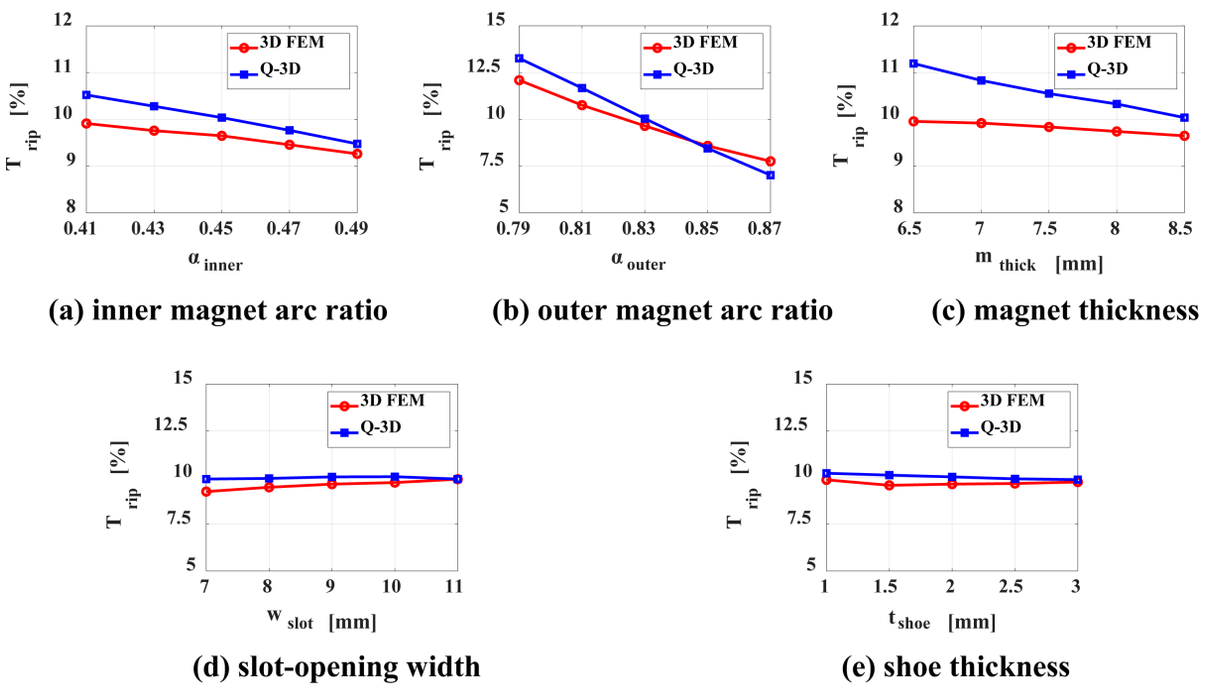


Fig. 6. (Color online) Comparison of torque ripple obtained using Q-3D and 3D FEM.

local electromagnetic-field effects near the slots that are not fully represented by the Q-3D model. Thus, Q-3D substantially reduces computational cost and captures several major design dependent trends of 3D FEM, although non-negligible fidelity differences remain for some output responses and design variables. In this study, Q-3D and 3D FEM are combined to achieve both low computational cost and high prediction accuracy of surrogate model.

Table 6. Correlation coefficients between the Q-3D and 3D FEM results for variations in individual design variables.

Number	Variable	Average torque	Torque ripple
①	α_{inner}	1.000	0.998
②	α_{outer}	1.000	0.998
③	m_{thick} [mm]	1.000	0.975
④	w_{slot} [mm]	0.981	0.275
⑤	t_{shoe} [mm]	0.999	0.258

3. Multi-Fidelity Surrogate Modeling Framework

3.1. Problem Definition

In this study, five design variables and two performance outputs are considered. The design variable vector is defined as

$$\mathbf{x} = [\alpha_{inner}, \alpha_{outer}, m_{thick}, w_{slot}, t_{shoe}]^T \quad (3)$$

where α_{inner} and α_{outer} are the inner and outer magnet arc ratios, m_{thick} is the magnet thickness, w_{slot} is the slot-opening width and t_{shoe} is the shoe thickness. The output vector is

$$\mathbf{y}(\mathbf{x}) = [T_{avg}(\mathbf{x}), T_{rip}(\mathbf{x})]^T \quad (4)$$

where T_{avg} and T_{rip} indicate the average torque and torque ripple, respectively. The low- and high-fidelity outputs are defined as

$$\mathbf{y}_L(\mathbf{x}) = [T_{avg,Q3D}(\mathbf{x}), T_{rip,Q3D}(\mathbf{x})]^T \quad (5)$$

$$\mathbf{y}_H(\mathbf{x}) = [T_{avg,3D}(\mathbf{x}), T_{rip,3D}(\mathbf{x})]^T \quad (6)$$

3.2. Data Sampling and Dataset Construction Method

Constructing an accurate surrogate model requires sufficient number of samples, and generating these samples can also incur considerable computational cost. Therefore, Latin hypercube sampling is employed in this study to improve sampling efficiency by effectively covering the design space with small number of samples.

Table 7. FEM data-generation time used for surrogate-model comparison.

Model	Q-3D samples	3D FEM samples	Computational time [s]
Q-3D-only	2195	0	368,760
3D FEM-only	0	100	368,800
TL model	1097	50	368,696
RC model	1097	50	368,696

Table 7 summarizes the data generation cost used to construct each surrogate model. In this study, the number of samples was determined based on a comparable computational budget. A single Q-3D and 3D FEM analysis requires 168 s and 3,688 s, respectively. The computational cost of 100 3D FEM analyses, corresponding to 368,800 s, was adopted as the reference budget. Under this budget, 2,195 Q-3D samples require 368,760 s. For the multi-fidelity models, 50 3D FEM samples and 1,097 Q-3D samples require 368,696 s, providing a comparable computational budget. The resulting datasets were subsequently divided into training and validation sets at a ratio of 80:20. In addition, the 50 samples in the independent 3D FEM test set are not used for model training, validation, or hyperparameter selection and are evaluated only after all model development is finalized [27]. The detailed sample construction is shown in Table 8.

3.3. DNN Based Surrogate and Comparison Models

During optimization, repeated analyses are required to identify the optimal design for different combinations of design variables. To reduce computational costs, surrogate model-based optimization has been widely studied [9-11]. A surrogate model is an approximate model that predicts the relationship between design variables and output variables. Because the surrogate model can efficiently predict model performance with low computational cost, replacing high computational cost FEM analyses with the surrogate model can significantly improve the computational efficiency of the optimization process.

Table 8. Model-development sample construction.

Model	Q-3D samples		3D FEM samples		
	Training data	Validation data	Training data	Validation data	Test data
Q-3D-only	1756	439	0		50
3D FEM-only	0		80	20	50
TL model	878	219	40	10	50
RC model	878	219	40	10	50

Table 9. DNN architecture and training hyperparameters.

Hyperparameter	Value	Hyperparameter	Value
Input neurons	5	Optimizer	Adam
Output neurons	2	Learning rate	1e-4
Hidden layers	3	Batch size	32
Units per hidden layer	32	Low-fidelity maximum epochs	2000
Activation function	ReLU	High-fidelity maximum epochs	2000

In this study, a deep neural network (DNN) is used to construct the surrogate model. The DNN consists of an input layer, one or more hidden layers, and an output layer. The input and output layers contain the same numbers of nodes as the design variables and output responses, respectively. Each hidden layer consists of multiple units with associated weights and biases, which are updated during DNN training to improve the prediction accuracy of the surrogate model. Because multiple hidden layers enable the DNN to learn nonlinear relationships between the inputs and outputs, the surrogate model can effectively represent the nonlinear relationship between the motor design variables and performances [26]. The DNN architecture and training hyperparameters used in this study are summarized in Table 9.

However, the performance of a single-fidelity surrogate model depends on the fidelity of the training data because the model is trained using only one type of data, such as Q-3D or 3D FEM data. To overcome this limitation, multi-fidelity surrogate models have been studied. These models combine low-fidelity Q-3D data with high-fidelity 3D FEM data to achieve high prediction accuracy while reducing computational cost.

The TL and RC models are used as multi-fidelity models in this study. To ensure a fair comparison, both models are constructed using the same sample composition and DNN architecture. First, the TL model is pre-trained using the Q-3D dataset to capture global trends of AFPM. Second, the pre-trained Q-3D surrogate model is fine-tuned using the 3D FEM samples. TL transfers the weights learned from a large low-fidelity dataset to improve the learning efficiency of a high-fidelity surrogate model. By fine-tuning the pre-trained model with small number of high-fidelity samples, TL can reduce the amount of computationally expensive high-fidelity data required for accurate surrogate modeling.

3.4. Multi-Fidelity Residual-Correction Surrogate Model

The overall training process of the RC model is illustrated in Fig. 1. First, many Q-3D samples are generated and used to train the Q-3D surrogate model. The initial weights and biases of the model are randomly initialized. At this stage, the Q-3D surrogate model is trained to capture the overall performance trends of the AFPM by taking advantage of the low computational cost of Q-3D. Second, a separate 3D FEM dataset containing small number of samples is generated. The differences between the 3D FEM results and the predictions of the Q-3D surrogate model are then used to train a residual surrogate model. The residual surrogate model is used to correct the predictions of the Q-3D surrogate model. Finally, the high-fidelity surrogate model is obtained by combining the Q-3D surrogate model with the residual surrogate model.

In this study, Q-3D is regarded as the low-fidelity model because it provides electromagnetic performance predictions at a much lower computational cost than 3D FEM by simplifying some three-dimensional magnetic effects. Based on the Q-3D samples, the low-fidelity dataset and the corresponding DNN surrogate model are defined as

$$\mathcal{D}_L = \{(\mathbf{x}_i^L, \mathbf{y}_L(\mathbf{x}_i^L))\}_{i=1}^{N_L} \tag{7}$$

$$f_L(\mathbf{x};\theta_L) \approx \mathbf{y}_L(\mathbf{x}) \tag{8}$$

To correct the difference between the low-fidelity surrogate predictions and the 3D FEM results, a high-fidelity development dataset is constructed using small number of 3D FEM samples. The high-fidelity development dataset is defined as

$$\mathcal{D}_H = \{(\mathbf{x}_j^H, \mathbf{y}_H(\mathbf{x}_j^H))\}_{j=1}^{N_H} \tag{9}$$

Using this high-fidelity dataset, the trained low-fidelity surrogate model is evaluated at each high-fidelity sample point. The model-level residual is then calculated as the difference between the corresponding 3D FEM result and the low-fidelity surrogate prediction. These residuals are used as training targets to construct the residual dataset and train a separate residual DNN surrogate model. The model-level residual for the *j*-th high-fidelity sample, the residual dataset, and the corresponding residual surrogate model are defined as

$$\boldsymbol{\delta}_M(\mathbf{x}_j^H) = \mathbf{y}_H(\mathbf{x}_j^H) - f_L(\mathbf{x}_j^H;\theta_L) \tag{10}$$

$$\mathcal{D}_\delta = \{(\mathbf{x}_j^H, \boldsymbol{\delta}_M(\mathbf{x}_j^H))\}_{j=1}^{N_H} \tag{11}$$

$$f_\delta(\mathbf{x};\theta_\delta) \approx \boldsymbol{\delta}_M(\mathbf{x}) \tag{12}$$

The model-level residual contains both the fidelity discrepancy between Q-3D and 3D FEM and the approximation error of the low-fidelity surrogate. The trained residual surrogate model predicts the correction required for the low-fidelity surrogate prediction. Accordingly, the proposed high-fidelity surrogate model is constructed by adding the predicted residual to the low-fidelity surrogate prediction and is defined as

$$\hat{\mathbf{y}}_H(\mathbf{x}) = f_L(\mathbf{x};\theta_L) + f_\delta(\mathbf{x};\theta_\delta) \tag{13}$$

To evaluate the prediction performance of the proposed RC model, the Q-3D-only, 3D FEM-only, and TL models are used as comparison models.

4. Surrogate Model Evaluation and Optimal Design

4.1. Prediction Performance Comparison of Surrogate Models

The prediction performance of all models is evaluated using the same 3D FEM test set. The performance of each surrogate model is evaluated separately for average torque and torque ripple using mean absolute percentage error (MAPE) and R^2.

$$MAPE = \frac{100}{N}\sum_{i=1}^{N}\left|\frac{y_i - \hat{y}_i}{y_i}\right| \tag{14}$$

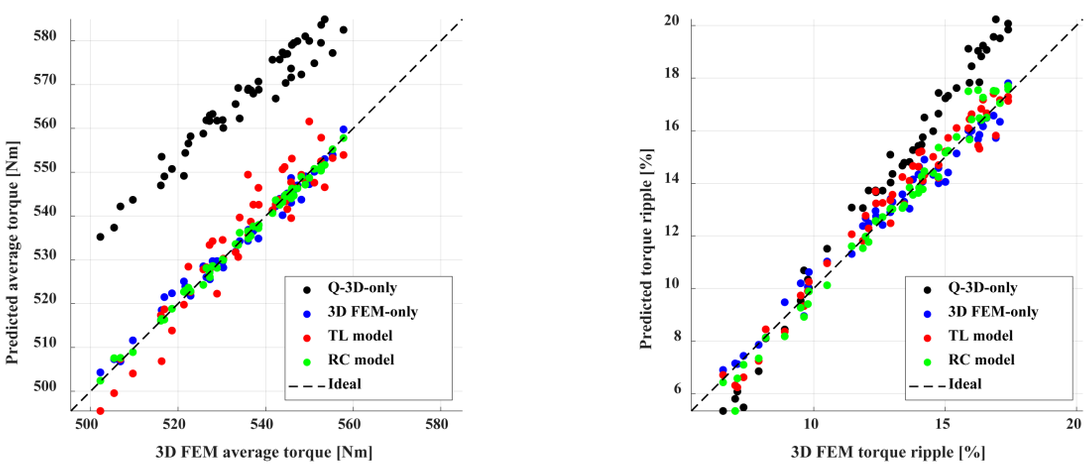
$$R^2 = 1 - \frac{\sum_{i=1}^{N}(y_i - \hat{y}_i)^2}{\sum_{i=1}^{N}(y_i - \bar{y})^2} \tag{15}$$

Table 10 summarizes the MAPE and R^2 values for average torque and torque ripple, and Fig. 7 compares the predicted and true 3D FEM results of average torque and torque ripple. In Fig. 7, predicted values located close to the ideal line indicate high prediction accuracy relative to the 3D FEM results.

For average torque, the Q-3D-only model shows overestimation in Fig. 7(a). Consequently, the Q-3D-only model obtains a MAPE of 5.85 % and a negative R^2 of −4.09. The TL model reduces the average torque prediction error by fine-tuning the Q-3D surrogate model using the 3D FEM dataset. During this process, fine-tuning corrects the difference between the Q-3D and 3D FEM results while maintaining the overall trend learned from Q-3D. However, when only small number of 3D FEM samples are available, it can be difficult to correct the difference between Q-3D and 3D FEM. Fine-tuning reduces the systematic error of the Q-3D-only model, showing a MAPE of 0.70 % and an R^2 of 0.88. However, the predictions remain more widely scattered than those

Table 10. Prediction performance on the common 3D FEM test set.

Model	Average torque		Torque ripple	
	MAPE [%]	R^2	MAPE [%]	R^2
Q-3D-only	5.85	-4.09	12.55	0.64
3D FEM-only	0.40	0.96	4.02	0.96
TL model	0.70	0.88	4.24	0.96
RC model	0.16	0.99	3.02	0.97



(a) average torque **(b) torque ripple**

Fig. 7. (Color online) Prediction performance plot on the common 3D FEM test set.

of the RC model, as shown in Fig. 7(a).

In contrast, the RC model keeps the Q-3D surrogate model fixed and directly learns the model-level residual between the Q-3D surrogate model prediction and the corresponding 3D FEM result. Therefore, the Q-3D surrogate model predicts the overall average torque trend, and the residual surrogate model corrects the remaining errors between Q-3D and 3D FEM. This direct correction generates predictions that are closer to the ideal line in Fig. 7(a). The proposed model achieves an average torque MAPE of 0.16 % and an R^2 of 0.99, outperforming both the TL model and the 3D FEM-only model.

The relationship between Q-3D and 3D FEM torque ripple is more dependent on the design variables than that observed for average torque. As shown in Fig. 6 and Table 6, the two methods exhibit similar trends for the magnet-related variables but considerably different trends for the slot-opening width and shoe thickness. Nevertheless, the Q-3D-only model captures the overall variation in torque ripple, although prediction errors remain, as shown in Fig. 7(b). Its MAPE and R^2 are 12.55 % and 0.64, respectively. Unlike the offset in average torque, the difference in torque ripple varies with the design and cannot be corrected by applying the same offset to all predictions.

The TL model performs comparatively well for torque ripple. Because the Q-3D and 3D FEM torque ripple values are generally similar, the pre-trained network can be fine-tuned using small number of 3D FEM samples. Therefore, the TL model achieves a torque ripple MAPE of 4.24 % and an R^2 of 0.96. The TL predictions are close to the ideal line in Fig. 7(b).

The proposed RC model nevertheless provides further improvement. Because the residual surrogate model directly learns the residual for each high-fidelity design point, it can capture both the overall output difference and changes in the relationship between Q-3D and 3D FEM across the design space. The proposed model achieves a torque ripple MAPE of 3.02 % and an R^2 of 0.97, compared with 4.24 % and 0.96 for the TL model and 4.02 % and 0.96 for the 3D FEM-only model. The RC model predictions are consequently distributed more closely around the ideal line in Fig. 7(b).

To further investigate the effect of the available computational budget, additional comparisons were performed between the 3D FEM-only and RC models. Table 11 summarizes the dataset configurations used in this analysis. Eight computational-budget cases were considered, corresponding to the computational cost of 30 to 100 3D FEM analyses. For the 3D FEM-only model, the entire computational budget was allocated to 3D FEM sample generation. For the RC model, approximately half of the computational budget was allocated to Q-3D samples and the remaining half to 3D FEM samples. Accordingly, the number of 3D FEM development samples for the RC model was varied from 15 to 50, while the number of Q-3D samples was varied from 329 to 1,097. The total data-generation costs of the 3D FEM-only and RC models were maintained at nearly the same level for each case. The 3D FEM development samples were divided into training and validation sets at a ratio of 80:20, and the same independent 3D FEM test set was used for all cases.

Table 11. Dataset configuration according to computational budget.

Case	3D FEM-only samples	RC model	
		Q-3D samples	3D FEM samples
1	30	329	15
2	40	438	20
3	50	548	25
4	60	658	30
5	70	767	35
6	80	877	40
7	90	987	45
8	100	1,097	50

Fig. 8 compares the prediction performance of the 3D FEM-only and RC models under the eight computational-budget cases. In general, the prediction accuracy of both models improves as the computational budget increases. However, the RC model consistently exhibits lower MAPE and higher R^2 than the 3D FEM-only model for both average torque and torque ripple over the entire range of computational budgets considered.

The difference is particularly evident under limited computational budgets. In Case 1, corresponding to the computational cost of 30 3D FEM analyses, the average-torque MAPE decreases from 1.26 % for the 3D FEM-only model to 0.33 % for the RC model, while the corresponding R^2 increases from 0.67 to 0.97. For torque ripple, the MAPE decreases from 8.05 % to 5.95 %, and R^2 increases from 0.84 to 0.92. These results indicate that the Q-3D data provide useful global response information when only a limited number of high-fidelity samples are available.

As the computational budget increases, the prediction performance of the 3D FEM-only model generally approaches that of the RC model because a larger number of high-fidelity samples becomes available. Nevertheless, the RC model maintains superior overall prediction performance throughout all eight cases. Therefore, the

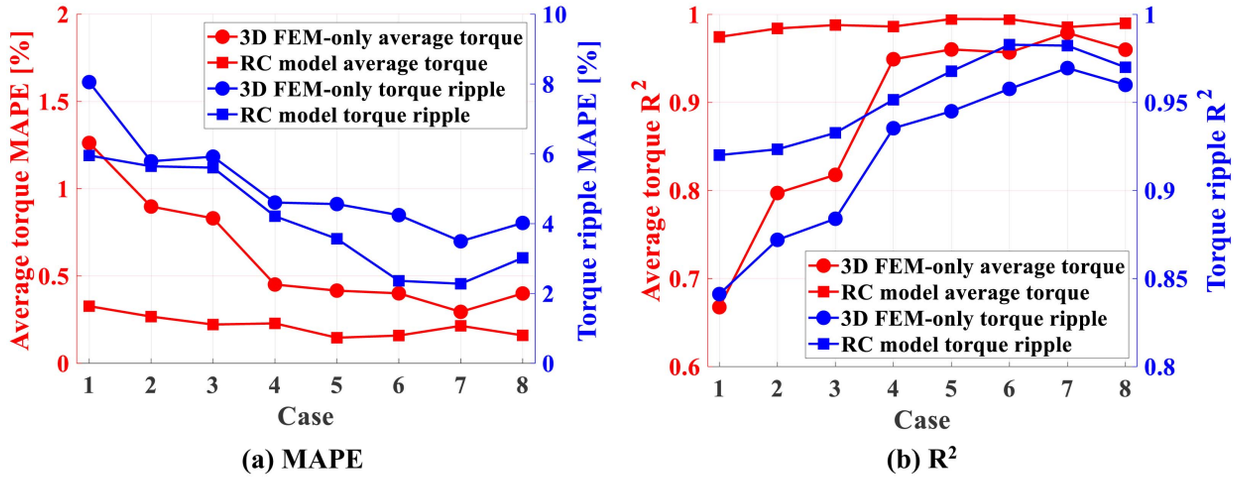


Fig. 8. (Color online) Prediction performance plot according to computational budget.

main advantage of the proposed multi-fidelity strategy is not that accurate prediction is impossible using only 3D FEM data, but that comparable or improved prediction accuracy can be achieved more efficiently, particularly when the availability of computationally expensive 3D FEM data is limited.

4.2. Optimization Problem and Genetic Algorithm

In this study, optimization is performed using a GA coupled with the surrogate model to reduce the computational cost associated with FEM. The GA settings used for optimization are summarized in Table 12. The optimal design obtained using the surrogate model and GA is then evaluated using 3D FEM. The 3D FEM results are used to evaluate the prediction error and verify that the objective and constraints are satisfied [10, 11].

To obtain an optimal design, this study uses a weighted sum objective function. The objective function is defined as

$$\min_{\mathbf{x}} F(\mathbf{x}) = \omega_T \frac{T_{avg,ref}}{\hat{T}_{avg,pred}(\mathbf{x})} + \omega_r \frac{\hat{T}_{rip,pred}(\mathbf{x})}{T_{rip,ref}} \tag{16}$$

$\hat{T}_{avg,pred}(\mathbf{x})$ and $\hat{T}_{rip,pred}(\mathbf{x})$ are the average torque and torque ripple predicted by the RC model, respectively, and $T_{avg,ref}$ and $T_{rip,ref}$ indicate the corresponding performance values of the initial model.

Table 12. Genetic algorithm settings.

Parameter	Value
Population size	10,000
Number of offspring per generation	5,000
Maximum number of generations	50
Mutation probability	0.3
Selection method	Roulette-wheel selection
Fitness scaling parameter	4

In AFPM design, average torque and torque ripple are two of the most important performance measures. Average torque determines the motor operating capability, and torque ripple affects motor noise and vibration. Therefore, in this study, the weights ω_T and ω_r are set to 0.5 to obtain a balanced trade-off between the two normalized performance measures.

The magnet volume constraint is

$$V_{mag}(\mathbf{x}) \le V_{mag,\text{initial}} \tag{17}$$

The magnet volume is limited to that of the initial model. This prevents performance improvement by simply using more permanent magnet material and allows a fair comparison of permanent magnet material usage.

4.3. Optimization and 3D FEM Verification

Table 13 summarizes the optimized design variables and compares the RC model predictions with the corresponding 3D FEM verification results. The RC model predicts an average torque of 553.22 Nm and a torque ripple of 5.10 %, and the 3D FEM evaluation obtains 553.63 Nm and 6.66 %, respectively. The prediction error for average torque is 0.07 % and torque ripple is 1.56 $\%_p$. Although the RC model shows high overall prediction accuracy for torque ripple, a prediction error of 1.56 $\%_p$ is observed at the selected optimal design. This difference is considered to be associated with the relatively complex and design dependent relationship between the Q-3D and 3D FEM torque ripple responses. As discussed in Section 2.4, the slot-opening width and shoe thickness exhibit relatively low correlations between Q-3D and 3D FEM

Table 13. Optimized design variables and comparison between the RC prediction and 3D FEM evaluation.

Variable	Initial model	RC prediction	3D FEM verification
V_{mag} [mm^3]	339,888	337,920	337,920
α_{inner}	0.45	0.42	0.42
α_{outer}	0.83	0.89	0.89
m_{thick} [mm]	8.5	8.1	8.1
w_{slot} [mm]	9	7.1	7.1
t_{shoe} [mm]	2	1.3	1.3
Average torque [Nm]	551.83	553.22	553.63
Torque ripple [%]	9.65	5.10	6.66

Table 14. Performance comparison between initial model and 3D FEM verification.

Variable	Initial model	3D FEM verification	Difference
V_{mag} [mm^3]	339,888	337,920	-0.58 [%]
Average torque [Nm]	551.83	553.63	+0.33 [%]
Torque ripple [%]	9.65	6.66	-2.99 [%$_p$]

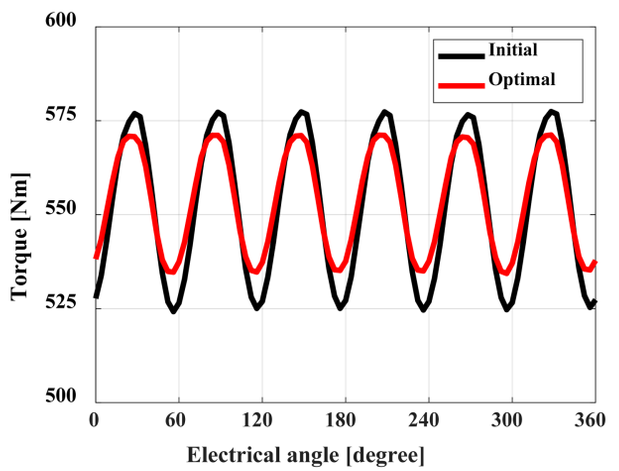


Fig. 9. (Color online) Torque waveform comparison of the initial and optimized models.

because local air-gap field harmonics and three-dimensional electromagnetic effects affecting torque ripple are not fully represented by the Q-3D model. Since the residual model is trained using a limited number of 3D FEM samples, these local variations may not be completely captured near the selected optimal design. As shown in Table 14, the optimized design increases the average torque by 0.33 %, reduces the torque ripple by 2.99 %$_p$, and reduces the magnet volume by 0.58 % compared with the initial model, satisfying the magnet volume constraint. The evaluated design also satisfies the rated torque and torque ripple requirements. Fig. 9 shows the torque waveform of the initial and optimal model. Although the 3D FEM torque ripple at the selected design is 1.56 %$_p$ higher than the RC prediction, it remains below the torque ripple target of 8 %.

5. Conclusion

This study proposes an RC multi-fidelity surrogate model for AFPM optimization by combining a Q-3D surrogate model with a separately trained residual surrogate model. Unlike TL, which fine-tunes the parameters of the low-fidelity model, the RC model directly learns the difference between the Q-3D surrogate prediction and the corresponding 3D FEM result. On the common 3D FEM test set, the proposed model achieves a MAPE of 0.16 % and an R^2 of 0.99 for average torque and a MAPE of 3.02 % and an R^2 of 0.97 for torque ripple, providing the best overall prediction performance among the models evaluated under the adopted dataset and computational cost conditions.

The RC model is subsequently coupled with a GA, and the selected optimal design is evaluated using 3D FEM. The evaluated optimal design satisfies the magnet volume constraint while maintaining the required average torque and reducing torque ripple. These results indicate that the proposed RC model can support AFPM optimization with computational efficiency.

The present study focuses on electromagnetic optimization considering average torque and torque ripple. The proposed RC framework can be extended to multiphysics optimization by incorporating additional responses and constraints, such as temperature and mechanical stress. In

future work, the proposed framework will be extended to include thermal and structural performance, and the optimized AFPM will be experimentally evaluated using a prototype to further validate the prediction and optimization results.

Acknowledgement

This work was supported by Korea Hydro & Nuclear Power Co and Local Government (Ulsan) (2026).

References

[1] W. Geng, Y. Fu, J. Wang, W. Li, and Y. Wang, IEEE Trans. Industrial Electronics **73**, 9606 (2026).
[2] Y. Zhou, J. Liu, Z. Chen, G. Yang, Y. He, A. Li, N. Kang, J. Chen, and C. H. T. Lee, IEEE Trans. Industrial Electronics **72**, 734 (2025).
[3] Z. Shi, X. Sun, Z. Yang, Y. Cai, G. Lei, J. Zhu, and C. H. T. Lee, IEEE Trans. Transportation Electrification **10**, 3770 (2024).
[4] N. Gadiyar, J. Van Verdeghem, and E. L. Severson, IEEE Trans. Industry Applications **59**, 3920 (2023).
[5] R. Huang, Z. Song, H. Zhao, and C. Liu, IEEE Trans. Transportation Electrification **8**, 2118 (2022).
[6] J. Feng, X. Fan, C. Ma, Y. Wang, and Z. Zhou, IEEE Trans. Transportation Electrification **12**, 6962 (2026).
[7] X. Yang, C. Cai, and Y. Zhao, IEEE Trans. Magnetics **62**, 7401305 (2026).
[8] N. Gori, C. Simonelli, A. Musolino, L. Sani, R. Rizzo, and H. Chen, IEEE Trans. Energy Conversion **41**, 1610 (2026).
[9] H. Sato and H. Igarashi, IEEE Trans. Magnetics **58**, 8202209 (2022).
[10] H. Zhang, G. Wang, J. Zhang, Y. Gao, W. Hua, and Y. Wang, IEEE Trans. Industry Applications **60**, 6799 (2024).
[11] S. Ahmed, C. Grabher, H.-J. Kim, and T. Koseki, IEEE Trans. Industrial Electronics **67**, 7280 (2020).
[12] Q. Li, A. Liu, and B. Zhang, IEEE Access **10**, 32022 (2022).
[13] M. Gulec and M. Aydin, IET Electric Power Applications **12**, 195 (2018).
[14] J.-M. Ahn, H.-K. Yeo, J.-Y. Kim, D.-H. Lee, and D.-K. Lim, IEEE Access **11**, 141241 (2023).
[15] K.-H. Kim and D.-K. Woo, IEEE Access **10**, 98842 (2022).
[16] H.-J. Oh, D. Cheo, S. H. Choi, S.-W. Jung, and S.-Y. Jung, J. Electrical Engineering & Technology **20**, 2201 (2025).
[17] J.-C. Son, D.-K. Lim, D.-H. Lee, P.-J. Kim, and H.-K. Yeo, J. Electrical Engineering & Technology **21**, 2691 (2026).
[18] J.-S. Lee, D.-K. Lim, D.-H. Lee, P.-J. Kim, and H.-K. Yeo, IEEE Access **13**, 64353 (2025).
[19] Y. Hwang, K.-O. Kim, W.-S. Cha, B.-C. Bae, J.-H. Kim, and M.-S. Lim, IEEE Trans. Magnetics **62**, 7500606 (2026).
[20] J. Wanjiku, M. A. Khan, P. S. Barendse, and P. Pillay, IEEE Trans. Industrial Electronics **62**, 7578 (2015).
[21] M. Aydin, Z. Q. Zhu, T. A. Lipo, and D. Howe, IEEE Trans. Magnetics **43**, 3614 (2007).
[22] J. Yang, J. Chen, W. Liu, G. Yang, and C. Zhang, J. Electrical Engineering & Technology **20**, 2277 (2025).
[23] S.-H. Park, J.-W. Chin, K.-S. Cha, and M.-S. Lim, IEEE Trans. Magnetics **58**, 8206005 (2022).
[24] M.-H. Sung, S.-H. Park, K.-S. Cha, J.-H. Sim, and M.-S. Lim, Machines **13**, 302 (2025).
[25] J.-H. Lee, S.-H. Park, D.-H. Park, J.-H. Jeong, and M.-S. Lim, IEEE Trans. Industry Applications **62**, 821 (2026).
[26] V. Parekh, D. Flore, and S. Schöps, IEEE Access **9**, 21786 (2021).
[27] G. C. Cawley and N. L. C. Talbot, J. Machine Learning Research **11**, 2079 (2010).